Graphene Polyimide Nanocomposites; Thermal, Mechanical, and High-Temperature Shape Memory Effects

Mitra Yoonessi,[†,*] Ying Shi,[⊥] Daniel A. Scheiman,[‡] Marisabel Lebron-Colon,[§] Dean M. Tigelaar,[†] R. A. Weiss,[⊥] and Michael A. Meador[§]

[†]Ohio Aerospace Institute, Cleveland, Ohio 44142, United States, [‡]ASRC, Cleveland, Ohio 44135, United States, [§]NASA Glenn Research Center, Cleveland, Ohio 44135, United States, and [⊥]Department of Polymer Enginneering, University of Akron, Akron, Ohio 44325, United States

ABSTRACT

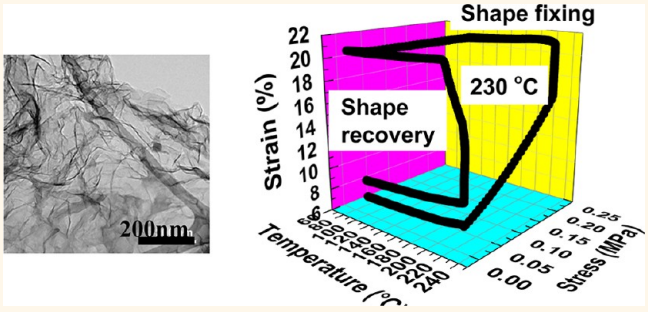

Flexible graphene polyimide nanocomposites (0.1−4 wt %) with superior mechanical properties over those of neat polyimide resin have been prepared by solution blending. Imide moieties were grafted to amine-functionalized graphene using a step-by-step condensation and thermal imidization method. The imide-functionalized graphene exhibited excellent compatibility with *N*-methyl-2-pyrrolidone. The dynamic storage moduli of the graphene polyimide nanocomposites increased linearly with increasing graphene content for both unmodified graphene and imidized graphene. Moduli of the imidized graphene nanocomposites were 25−30% higher than those of unmodified graphene nanocomposites. Both neat polyimide and polyimide nanocomposites exhibited shape memory effects with a triggering temperature of 230 °C. where addition of graphene improved the recovery rate. Addition of graphene improved thermal stability of the polyimide nanocomposites for both graphene and modified graphene.

KEYWORDS: graphene · polyimide nanocomposites · shape memory polymers · mechanical properties · thermal stability · exfoliation

Graphene is a sp^2-bonded monatomic thick quasi-two-dimensional nanoparticle consisting of fused six-membered carbon rings with micrometer-sized lateral dimension. It was first reported as a free-standing nanoparticle by Geim and co-workers in 2004.[1−5] The nonlinear stress−strain elastic response of a graphene membrane exhibited second- and third-order elastic constants of 340 and −690 N/m, respectively, and a breaking strength of 42 N/m, which corresponds to a Young's modulus of 1 TPa, a third-order elastic stiffness of $D = -2$ TPa, and an intrinsic strength of 130 GPa for bulk graphite.[6] Graphene obtained from the reduction of graphene oxide resulted in a Young's modulus of $E = 0.25$ TPa and lower tension bending compared to mechanically exfoliated graphene.[7]

Highly aromatic polyimide resins have high thermal stability (>300 °C), high glass transition temperature (T_g > 200 °C), high tensile strength, low creep, excellent radiation shielding capability, flexibility, and low color, which make them attractive materials for aeronautics and space structural components.[8] Nanoparticles can be added to polyimides to improve their mechanical and physical properties. The addition of aliphatic/aromatic dispersants to a mixture of single-wall carbon nanotubes (SWNTs) results in improved dispersion of SWNTs in the matrix.[9] The tensile properties of vapor-grown carbon nanofiber (VGCF)/polyimide (CP2) nanocomposites prepared by *in situ* grafting of a surface-modified VGCF were superior to those of a simple blend.[10] Polyimide containing double-decker-shaped silsesquioxane, POSS, in the main chain exhibited a low dielectric constant, high thermal stability, good solubility, T_g > 300 °C, and high modulus and strength.[11] Clay hybrid polyimide nanocomposites prepared by the addition of layered silicate to an alkoxy-terminated amide acid oligomer and tetraethoxysilane are 300% stiffer above T_g and 30% stiffer at room temperature compared to the neat polyimide.[12] Covalent bonding of a mesoporous silica with polyimide produced a 160% increase in modulus, 37.5 °C increase in thermal decomposition temperature, and 14.5 °C increase in T_g.[13] Incorporation of silver acetate in the polymerization of polyimide resulted in films

* Address correspondence to mitra.yoonessi@gmail.com.

Received for review March 4, 2012 and accepted August 21, 2012.

Published online August 29, 2012
10.1021/nn302871y

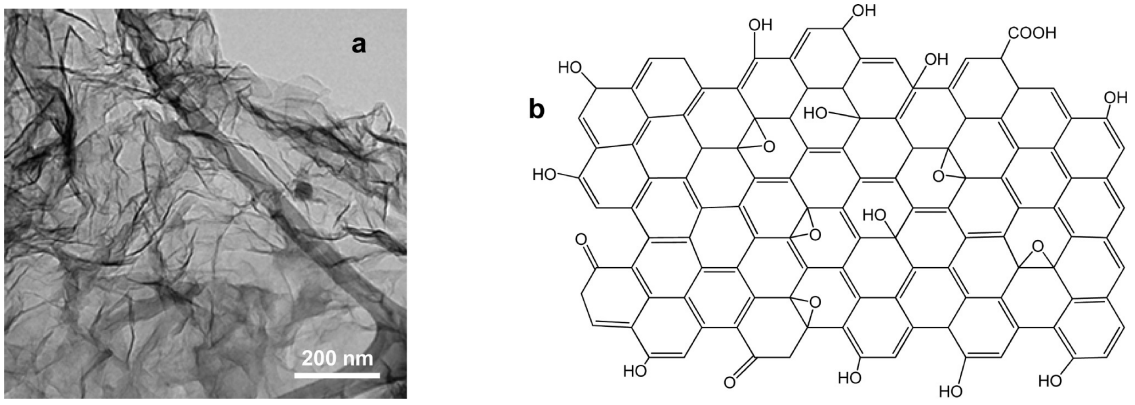

Figure 1. (a) HR-TEM of folded graphene with defects. (b) Postulated chemical structure of oxygenated graphene.

with high conductivity and reflectivity suitable for radiation applications.[14] Surface modification of SWNTs with 1-pyrene-4-(*N*′-5-norbornene-2,3-dicarboximide) improved the dispersion of the CNTs in the polyimide resin matrix and enhanced the tensile strength and the electrical conductivity.[15]

The properties of polymer nanocomposites depend on the nanoparticle characteristics, aspect ratio, and the extent of nanoparticle dispersion. Nanoparticles agglomerate due to van der Waals forces, which depend upon the geometry and separation distance between the nanoparticles, for example, for plates $W = -A/12\pi D^2$, where A is the Hamaker constant and D is the plane separation.[16] The extremely high aspect ratio and high surface area of graphene contribute to the larger Hamaker constant and higher attractive van der Waals forces. Aggregation of nanoparticles results in poor physical and mechanical properties in polymer nanocomposites if the aggregates act as stress concentration points.

Thermally responsive shape memory polymers and polymer nanocomposites are materials that mechanically respond to an external stimulus of thermal energy. When stress is applied at a temperature higher than the critical temperature, T_c, the material deforms to a temporary shape which is recoverable by applying thermal energy.[17−19] This critical temperature is influenced by T_g, the crystallization temperature, physical cross-links, or light chemical cross-links. The bulk of the research to date on thermally responsive shape memory polymers has been focused on low and medium use temperature elastomeric polymers, such as thermoplastic polyurethane elastomers (TPU),[19] cross-linked polyethylene,[20] sulfonated EPDM,[21] and polynorbornene,[22] for applications such as biomedical and surgical materials, smart fabrics, and heat-shrinkable tubing. Recently, ultralow concentration of graphene was dispersed in diamine to form highly dipsersed graphene epoxy nanocompsite shape memory polymers.[23,24] These graphene epoxy nanocomposites exhibited enahnced self-healing properties with ultralow graphene contentration at 90 °C.[23,24] However, aerospace structural components, especially those in propulsion systems, require high switching temperatures. To the best of our knowledge, there is no report of a shape memory polymer suitable for use at temperatures above 200 °C.

Herein, we report the preparation, superior thermal mechanical properties, and high-temperature shape memory effects of polyimide and polyimide graphene nanocomposites using reduced graphene and surface-imidized graphene. Surface imidization resulted in highly stable dispersions of graphene in *N*-methyl-2-pyrrolidone (NMP). Attempts were made to correlate the morphology of the graphene nanoparticles in the polyimide to the thermal and mechanical properties.

RESULTS AND DISCUSSION

Graphene. Exfoliated graphene nanosheets used in this study were prepared by the rapid high-temperature thermal decomposition of graphene oxide prepared as reported by Aksay *et al.*[25−27] These graphene nanosheets had lateral dimensions between 700 nm and 15 μm (3 μm average) as measured by high-resolution TEM.[28] Large wrinkling with peak heights of 10 nm has been observed by AFM and has been attributed to artifacts of both oxidation and reduction processes.[25] Figure 1 shows a HR-TEM image of the reduced graphene with 7% atomic oxygen content by XPS.[28] Graphene nanosheets prepared by this method have high oxygen content and different oxygenated functional groups.[25−27] The graphene nanosheets have folded architectures wherein the folding and strain are partially attributed to the presence of strained expoxide groups within the graphene plane.[25] Rearrangement of six-membered carbon rings to molecular kinks such as 5-8-5 also results in folding.[25,26] This highly oxygenated graphene (O-graphene) can be reduced chemically to generate sp^2-hybridized graphene with few oxygenated groups.

Graphene Surface Modifications. Highly oxygenated graphene nanosheets contain hydroxyl groups which can readily react with methoxy groups of *p*-phenylene

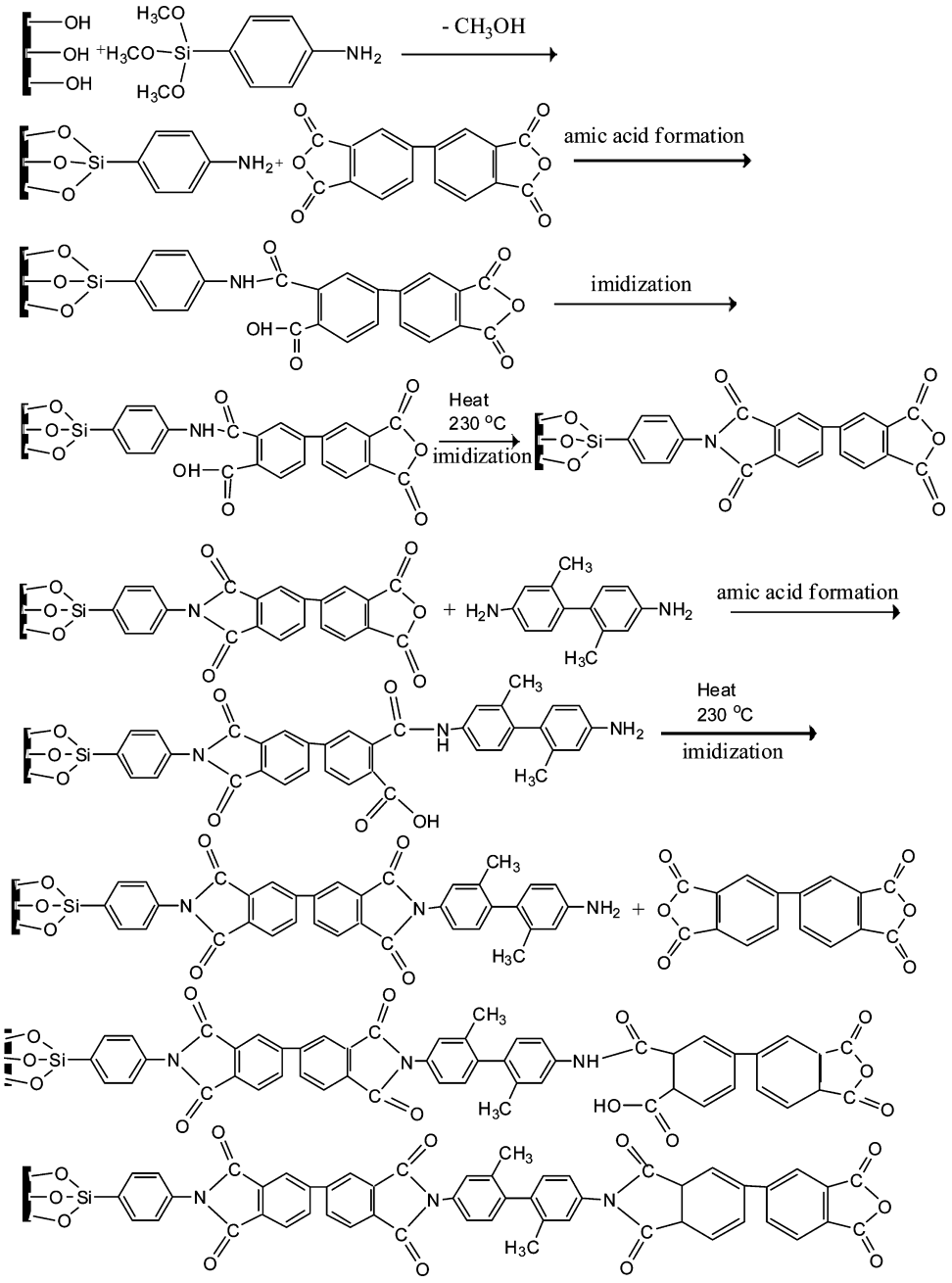

Figure 2. Reaction scheme of surface imidization of graphene.

trimethoxyaminosilane (Figure 2). Surface treatment of O-graphene with *p*-phenylene trimethoxyaminosilane results in a thermally robust functionalized graphene with amine end groups, due to the presence of both high thermally stabile aromatic moieties and Si–O bonds anchoring the functionality to the graphene surface.

Graphene Surface Characterization. *IR.* The IR spectrum of the *p*-phenylene trimethoxyaminosilane-modified graphene shows the –N–H stretch from the $-NH_2$ terminal group at 3431 cm^{-1}, CH_2 and CH_3 stretches at 2920 and 2851 cm^{-1}, the C=C stretch of the benzene ring at 1590 cm^{-1}, and the Si–O stretch at 1098 cm^{-1} (Figure 3a).[29] Treatment of this amine-terminated graphene with s-BPDA followed by thermal imidization at 230 °C produces an imide-functionalized graphene as confirmed by the presence of imide carbonyl peaks at 1771 and 1720 cm^{-1}, imide C–N–C bond at 1345 cm^{-1}, imide C–N bond at 1248 cm^{-1}, and Si–O at 1081 cm^{-1} (Figure 3b) in the infrared spectrum. The unreacted anhydride terminal groups in this material were further reacted with *m*-tolidine and imidized at 230 °C. The infrared spectrum of this material revealed imide carbonyl peaks at 1724 and 1775 cm^{-1}, imide C–N–C at 1368 cm^{-1}, imide C–N at 1250 cm^{-1}, and Si–O at 1094 cm^{-1}, consistent with the formation of additional imide groups (Figure 3c). This step was

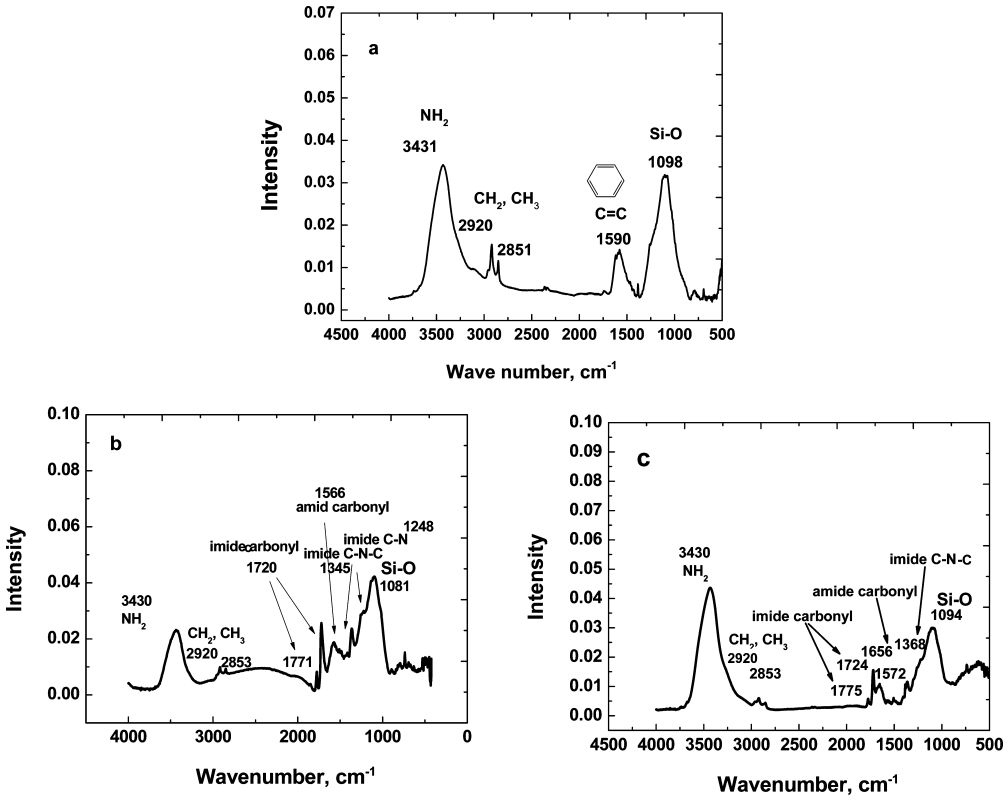

Figure 3. Infrared spectra of (a) graphene modified with *p*-phenylene trimethoxyaminosilane, (b) amine-terminated graphene reacted with anhydride group of *s*-BPDA dianhydride, (c) anhydride-terminated graphene reacted with amine group of *m*-tolidine.

repeated to bond four monomer units to the graphene surface.

TGA. The graphene nanoparticles that were surface-modified with imide moieties had improved thermal stability over oxygenated graphene (Figure 4). Oxygenated graphene exhibited a 6 wt % weight loss due to the decomposition of functional groups such as hydroxyls, epoxides, carboxylic acids, and phenolic hydroxyls. This decomposition starts at 47 °C and continues up to 340 °C. The onset of graphene decomposition was at 496 °C. Decomposition was rapid with the temperature of the maximum decomposition rate occurring at 663 °C. While the organic surface modifier on the imide surface-functionalized graphene started to decompose at 285 °C, the overall weight loss up to 1000 °C is gradual and much less severe with ~4% weight loss starting at 285 °C up to 393 °C followed by steady weight loss up to 1000 °C.

XPS. Imidized Graphene. The calculated atomic percentages of the constituent elements in the imide-functionalized graphene based on high-resolution X-ray photoelectron spectroscopy was C 1s 84.9%, O 1s 10.7%, N 1s 2.8%, Si 2p 1.3%, and S 2p 0.4%. The atomic percentage of the oxygen increased significantly compared to pristine graphene due to imide functionalization. Nitrogen was present due to imide bonds, and silicon was present at the connecting bond between the imide modifier and the graphene from

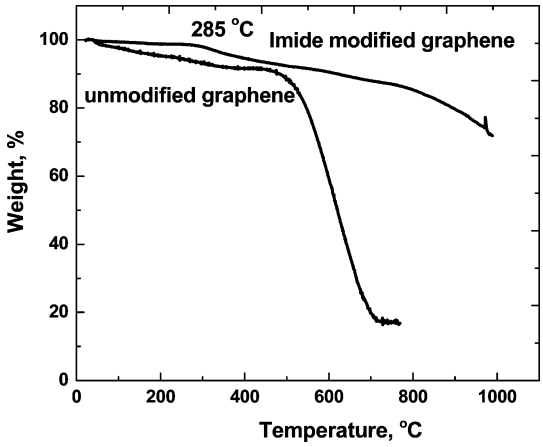

Figure 4. TGA of oxygenated graphene and imide-modified graphene.

the *p*-phenylene trimethoxyaminosilane reaction with graphene. The presence of sulfur is most likely due to residual impurities from the acid treatment.

Deconvolution of the oxygen peaks in the spectrum revealed peaks at 531.34, 532.20, 533.44, and 538.65 eV. The Si−O−C oxygen appears at 531.40 eV, which is due to the covalent bonding of the methoxysilane to the graphene surface.[30] The peak at a binding energy of 532.3 eV is due to the imide carbonyl oxygen.[31] The oxygen peak with a binding energy of 533.41 eV can be attributed to either hydrolysis of

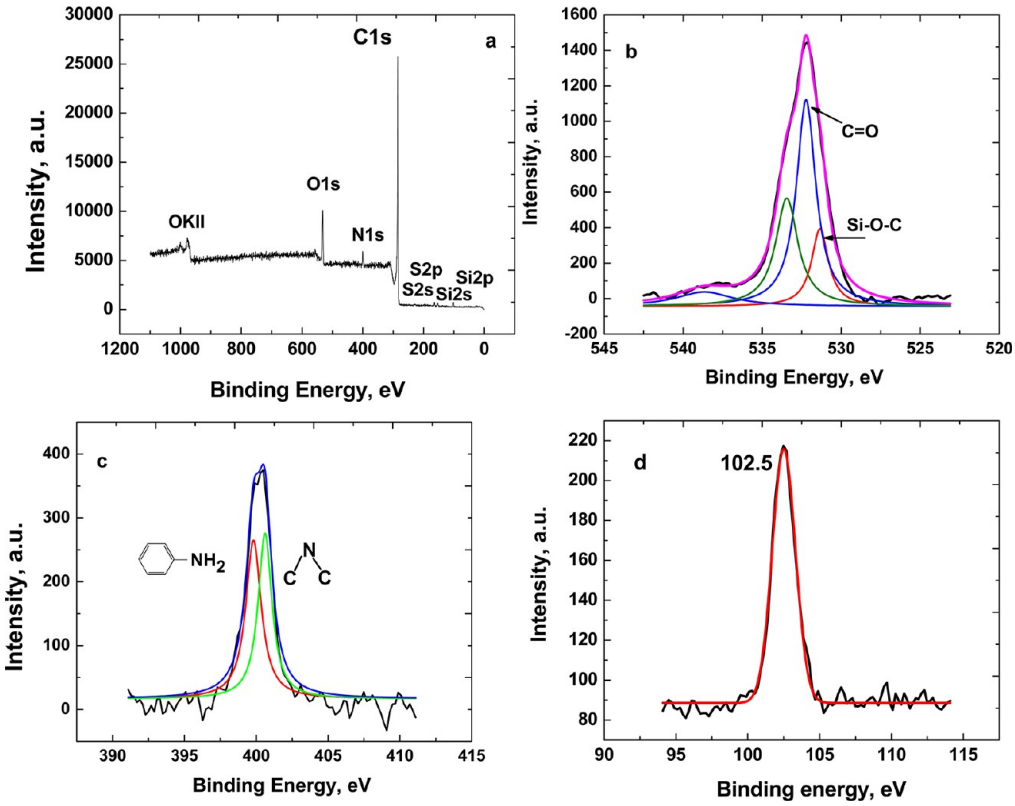

Figure 5. (a) Survey spectra of the surface imidized graphene. Experimental high-resolution and deconvoluted peaks (b) oxygen; (c) nitrogen and (d) silicon.

methoxy groups to SiO_2[30] or the shift of the carboxyl C═O close to the graphene surface due to the presence of an electron-donating silicon atom.[30] The high binding energy peak of 536.5 eV is a O 1s, due to the Si−O.

For nitrogen, peaks at binding energies of 399.91 and 400.65 eV can be assigned to the phenylene amine[31] and imide nitrogen atoms, respectively (Figure 5).[32]

Dispersions of Surface-Modified Graphene. Figure 6 shows dispersions of 5 mg/10 cm^3 O-graphene and imide surface-functionalized graphene in NMP after 3 months. The O-graphene precipitated prematurely due to poor interactions between the O-graphene and NMP. NMP is highly polar and interacts with polyamic acid. Enhanced interactions between the nanoparticles and the solvent resulted in longer stability of the graphene in NMP dispersions.

Polyimide Nanocomposites. *Polyimide Synthesis.* Polyimide was prepared from polycondensation of BAPP and BPADA (Figure 7).[15] A stoichiometric ratio of BAPP and BPDA was used to achieve the highest molecular weight. Generally, polyimide synthesis in dipolar aprotic solvents under strict dry conditions is a two-step process involving the instantaneous formation of poly(amic acid) at low temperature followed by imidization of the poly(amic acid) intermediate at high temperatures with formation of water as a byproduct.

The BAPP/BPADA polyimide produces films that are semitransparent, flexible, and have high thermal stability (onset of decomposition >500 °C). The ether linkage in the polyimide backbone provides some degree of flexibility to the highly aromatic polyimide structure. Pendant dimethyl groups attached to the bisphenol A portion of the backbone also contribute to increased flexibility, increased free volume, and help to render the polyimide soluble in common organic solvents such as chloroform, dichloromethane, NMP, and THF. The large monomer structure consisting of several aromatic rings allows formation of higher molecular weight polymers more rapidly. The molecular weight of the polyimide was M_n = 29 000 g/mol, M_w = 65 000 g/mol, and polydispersity of 2.2 measured by size exclusion chromatography (SEC).

Graphene Polyimide Nanocomposites. *Thermal and Mechanical Properties.* Figure 8 shows the dynamic tensile storage moduli, E', of polyimide and graphene polyimide nanocomposites (0.1−4 wt %). The storage modulus of the nanocomposites increased with increasing graphene content below glass transition temperature (Figure 8a). This effect is indicative of the reinforcement effects of the graphene in the polyimide resin. The increase in the modulus in the rubbery state was not significant and only observed for 2 and 4 wt % graphene polyimide nanocomposites. The tan δ of the nanocomposites exhibited a maximum of 212 ± 3 °C corresponding to the T_g of the

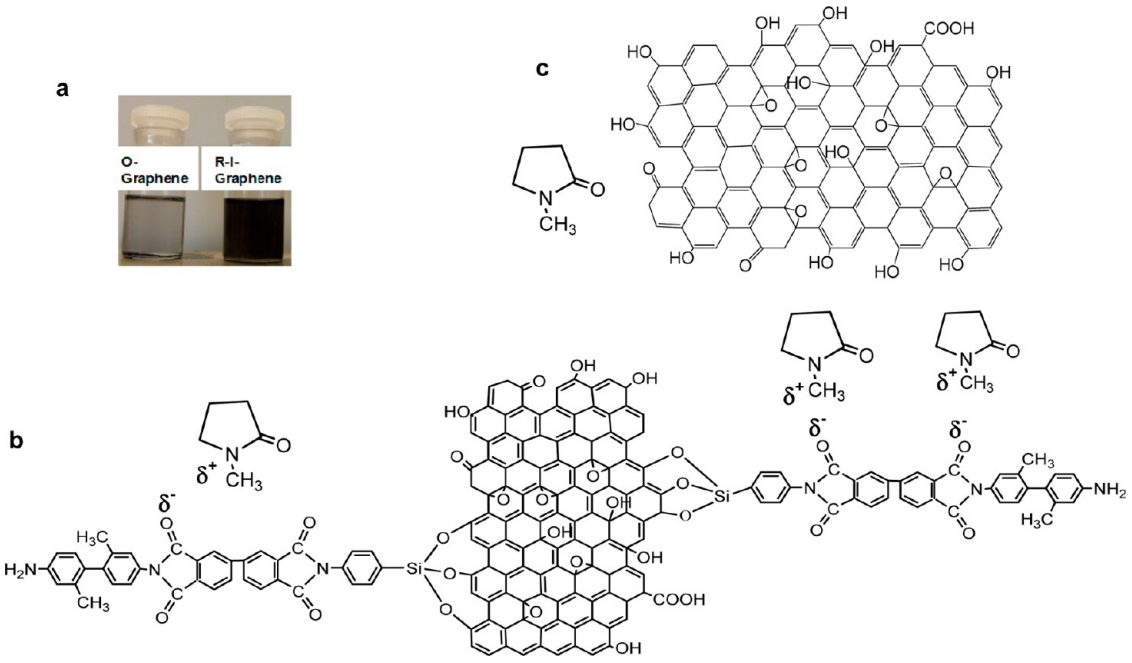

Figure 6. (a) Dispersion of unmodified graphene in NMP compared to the dispersion of the rigid imidized graphene in NMP after 60 days. (b) Structure of the rigid imide surface modifier covalently bonded to graphene. (c) Oxygenated graphene with NMP.

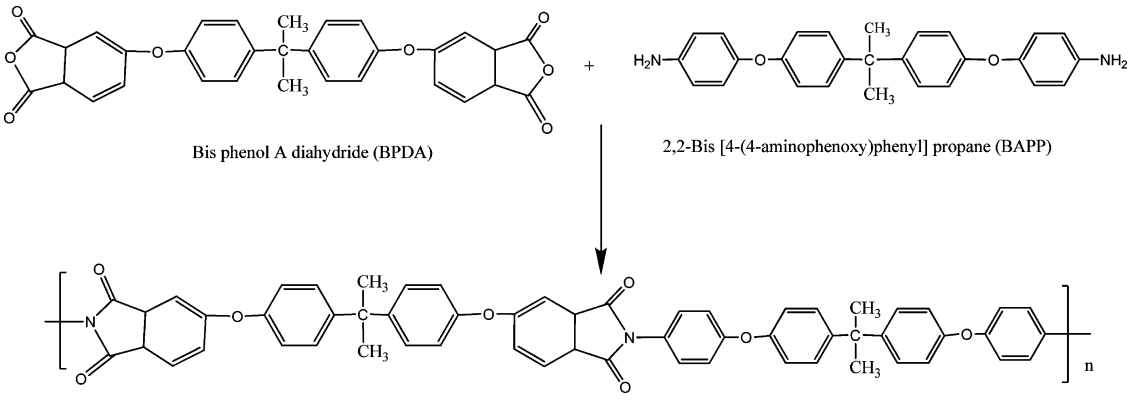

Figure 7. Schematics of polycondensation reaction of BAPP and BPADA resulting polyimide.

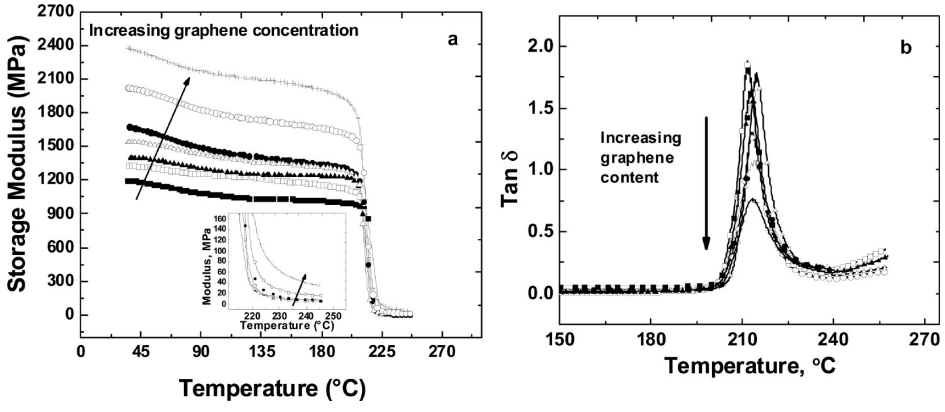

Figure 8. (a) Dynamic tensile moduli of polyimide and graphene polyimide nanocomposite as function of graphene content. (b) Tan δ of the polyimide and graphene polyimide nanocomposites: (■) polyimide, (□) 0.05 wt %, (▲) 0.1 wt %, (△) 0.5 wt %, (●) 1 wt %, (○) 2 wt %, (+) 4 wt % graphene polyimide nanocomposites.

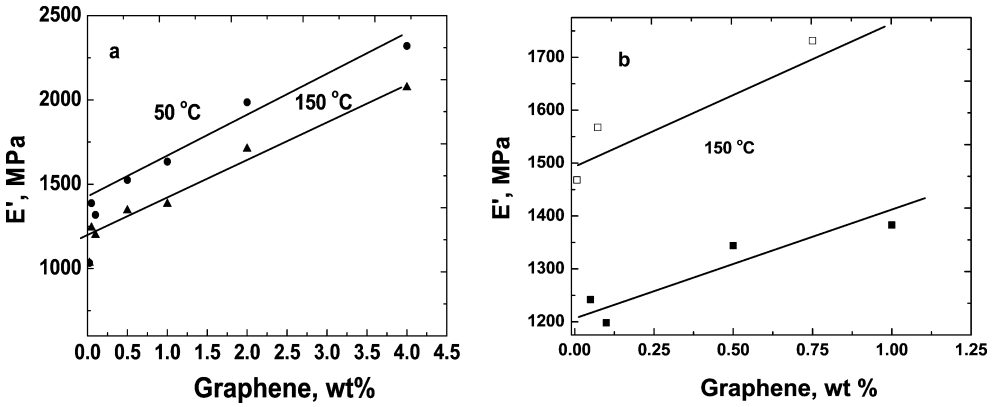

Figure 9. (a) Dynamic tensile moduli of graphene polyimide nanocomposites at 50 (●) and 150 °C (▲) as a function of graphene content. (b) Dynamic storage moduli of the polyimide nanocomposites containing graphene (■) and rigid imidized graphene (□) at 150 °C.

polyimide and graphene polyimide nanocomposites (Figure 8b). Presence of graphene did not affect the glass transition temperature. However, the area under damping peak (tan δ) was decreased with increasing graphene content. As previously reported, nanocomposites of graphene/polycarbonate[28] also did not exhibit significant changes in glass transition temperature when graphene was added to the polycarbonate. Graphene polycarbonate nanocomposites also exhibited a decrease in the area under the damping peak. This can be attributed to the weak attractive forces between the graphene and the polyimide resin matrix, which are insufficient to hinder segmental motion of the polymer chains.

The storage moduli of the graphene polyimide nanocomposites at 50 and 150 °C were plotted as a function of nanocomposite graphene content (Figure 9a). The moduli of graphene polyimide nanocomposites increased with increasing graphene content linearly. The storage moduli of the graphene polyimide nanocomposites containing reduced graphene are compared with the nanocomposites containing rigid imide surface-modified graphene (Figure 9b). The storage moduli of the surface-imidized graphene nanocomposites were 25−30% higher than those containing only reduced graphene. The storage moduli increased linearly with increasing graphene content. The increase in modulus is attributed to both improved dispersion of graphene in the polyimide resin matrix and the presence of surface modifier containing the stiffer benzene rings.

Thermal Stability. The onset of thermal decomposition, $T_{d,95}$, of the graphene of the polyimide graphene nanocomposites increased with increasing graphene content (Figure 10). A T_d value of 504 °C was measured for the neat polyimide, whereas T_d values for all of the graphene polyimide nanocomposites were higher and increased with increasing graphene content. While addition of both

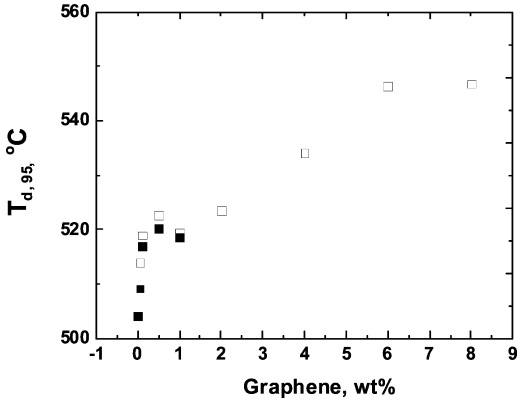

Figure 10. Thermal stability of graphene polyimide (□) and RI-graphene polyimide (■) nanocomposites.

surface-modified graphene and unmodified graphene resulted in improvements in the thermal stability, there is no apparent advantage to using surface-modified graphene.

Shape Memory. Figure 11a−e shows the sequence of a typical shape memory cycle. The polymer (polymer nanocomposite) has an initial length of L_1 at room temperature. The polymer is heated to a temperature above triggering temperature (*i.e.*, glass transition temperature). A stress is applied at $T > T_g$, where the length is increased to $(L_1 + \Delta L)_1$ (Figure 11b,c). The temperature decreased, and then the stress is removed. At this stage, the length was changed to $(L_1 + \Delta L)_2$ and the new shape is fixed (Figure 11d). This is a temporary shape, and the polymer will return to its original shape upon heating up to the glass transition temperature. The recovery is 100% if the polymer (polymer nanocomposites) returns to its full original length $L_1 = L_2$.

The strain recovery rate, R_r, is the ability of the materials to recover to its permanent shape,[17−19] and the ability of the switching segments to hold the applied mechanical deformation during this process is called the strain fixity rate, R_f.[17] The strain recovery

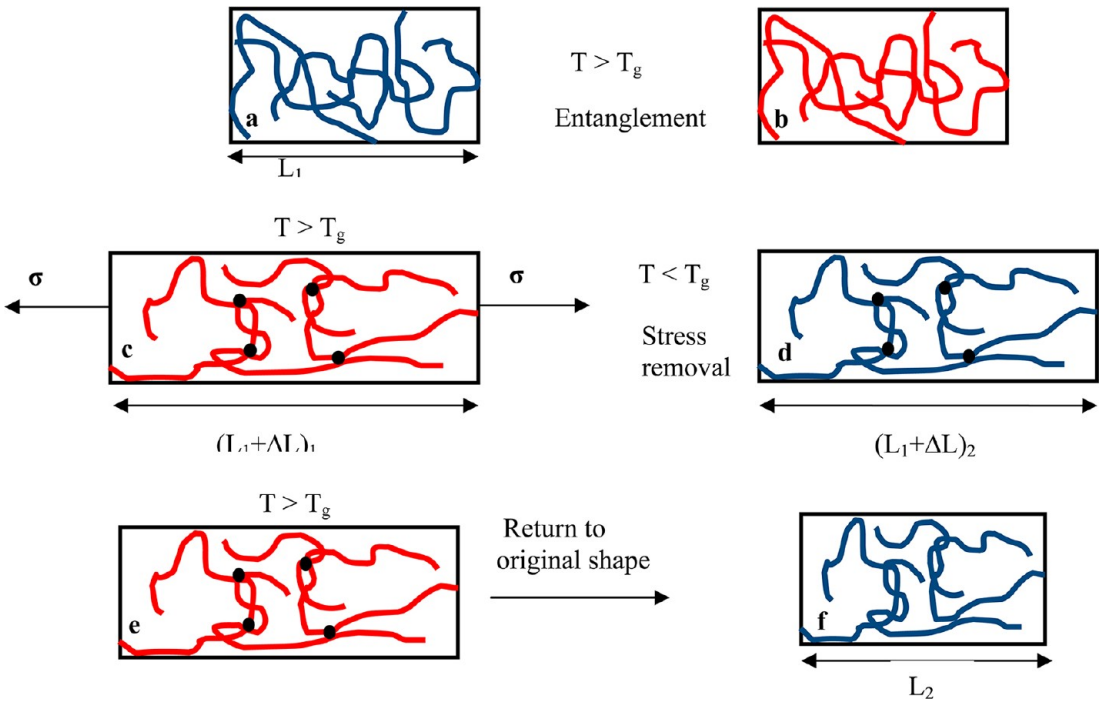

Figure 11. Schematics of shape memory behavior when T_g is used as a switching temperature. The polymer (polymer composite) has 100% recovery if $L_1 = L_2$.

rate is calculated using $R_r = \varepsilon_m - \varepsilon_p(N)/\varepsilon_m - \varepsilon_p(N-1)$, where ε_m is mechanical deformation and $\varepsilon_p(N)$ the permanent shape after N cycles.[17] The strain fixity rate is calculated using $R_f = \varepsilon_u(N)/\varepsilon_m$, where $\varepsilon_u(N)$ is the residual of strain after retraction in the nth cycle.[17] The triggering temperature can be a crystallization temperature, glass transition temperature, or the temperature at which a physical cross-link reverses.[17−19] In this study, the triggering temperature is glass transition temperature, T_g.

Figure 12 shows the three-dimensional shape memory behavior of the neat polyimide, where the glass transition temperature was used as the triggering temperature. The parameters were calculated based on the strain values in the third cycle. The neat polyimide showed a large deformation in the first cycle. A viscous plastic deformation of 5% was observed when neat polyimide is under stress at high temperature. This deformation was larger in the first cycle and reduced in the next cycles. The third cycle mechanical deformation, ε_m, was 21.2%. The neat polyimide showed a strain recovery rate of 89% after the third cycle and shape fixity rate of 97% (Figure 12a,a-1). Figure 12b,b-1 shows the stress−strain−temperature behavior for the 0.5 wt % graphene polyimide nanocomposites. The viscous deformation decreased to ∼3% with addition of graphene. The third cycle mechanical deformation was 14.2%. The strain recovery rate and strain fixity rate were improved with addition of graphene where a 0.5 wt % graphene polyimide nanocomposite exhibited R_r of 95% and R_f of 95%. Figure 12c,c-1 demonstrates the stress−strain−temperature behavior of 1 wt % graphene polyimide nanocomposite. The initial viscouse deformation remained in the same range of ∼3%. The third cycle mechanical deformation was 18.3%, which is lower than the neat polyimide but higher than the 0.5 wt % graphene polyimide nanocomposite. The strain recovery rate and strain fixity rate were improved to the level of R_r of 96% and R_f of 96%. The strain recovery rate and strain fixity rate had significant improvement compared to the neat polyimide resin when graphene nanoparticles were added to the polyimide. A large improvement was observed when 0.5 wt % graphene was added; meanwhile, further increase of graphene content to 1 wt % only resulted in 1% improvement in strain recovery rate and strain fixity rate.

HR-TEM. HR-TEM images of the 0.5 wt % graphene polyimide nanocomposites and surface-imidized graphene polyimide nanocomposites are shown in Figure 13. Both unmodified and surface-imidized graphene were well-dispersed in the polyimide resin matrix. Graphene was dispersed as a mixture of mono-, bi-, and multilayer small stacks containing few graphene nanosheets. The resolution of images was insufficient to provide accurate number of layers per stacking. Well-expanded small stacks along with well-exfoliated graphene nanosheets are evident in Figure 13a and appear to be bent and curved. The surface-imidized graphene also had good dispersions in the polyimide resin matrix forming small tactoids

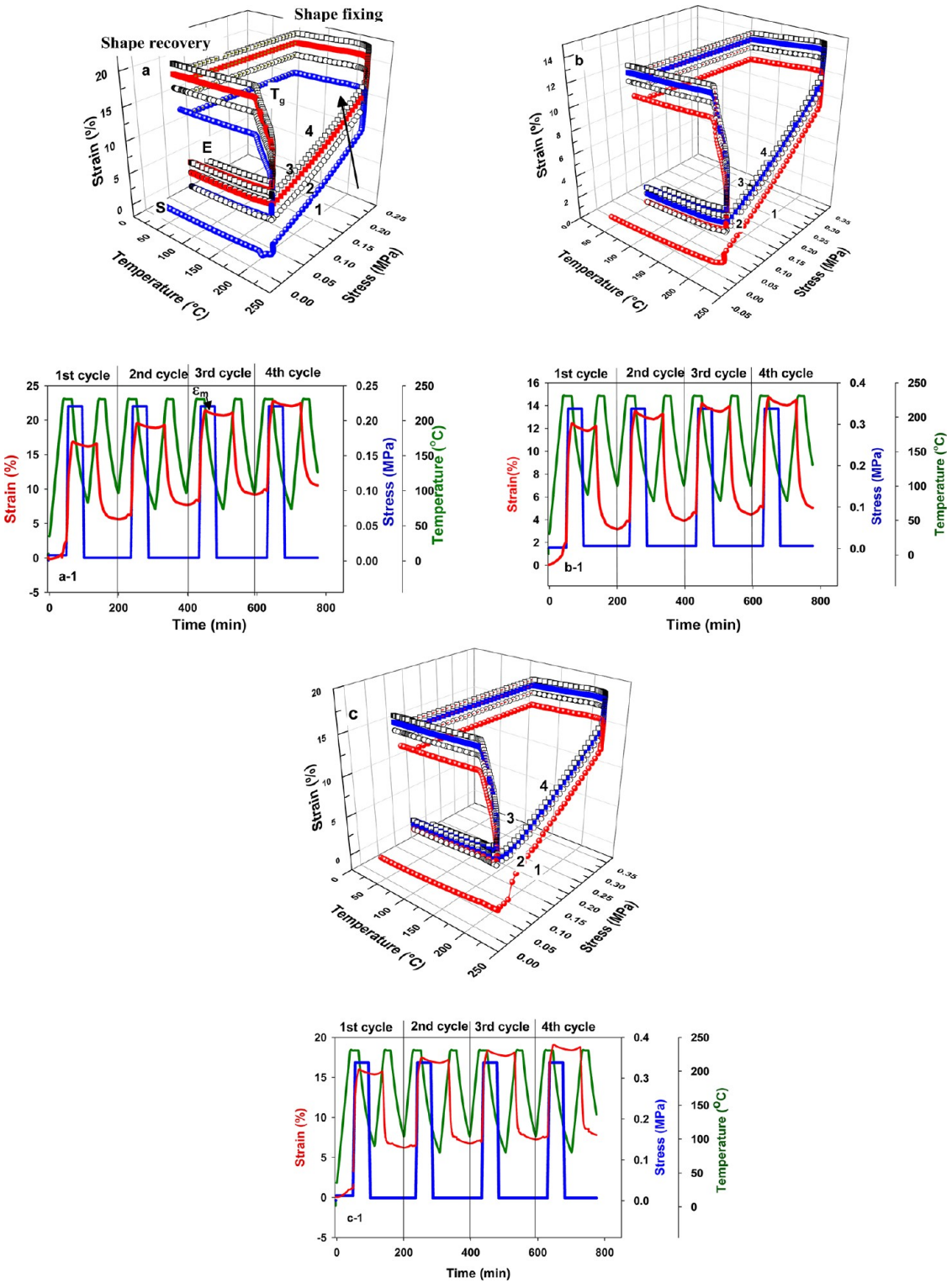

Figure 12. (a) Three-dimensional shape memory stress−strain−temperature data of (a) neat polyimide, (b) 0.5 wt % polyimide graphene nanocomposite, and (c) 1 wt % polyimide graphene nanocomposite. Two-dimensional demonstration of change of strain, stress, with temperature and time (a-1) neat polyimide, (b-1) 0.5 wt % polyimide graphene nanocomposite, (c-1) 1 wt % polyimide graphene nanocomposite.

and exfoliated graphene nanosheets. These graphene sheets have less bending and curvature possibly due to the stiff imide surface modifier. The graphene polyimide interface exhibited a higher contrast with the polyimide resin matrix (Figure 13c,d). This was not visible around the interface of the unmodified graphene in the graphene polyimide resin matrix. We attribute this contrast to the imide surface modifier

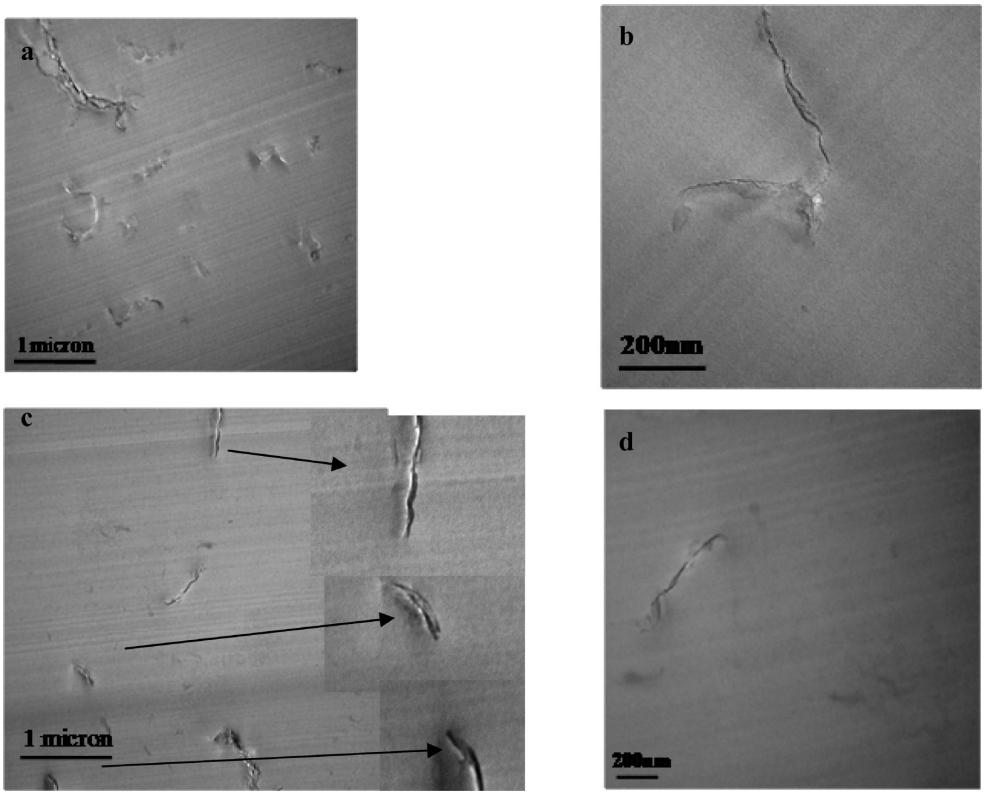

Figure 13. Transmission electron micrographs of the polyimide graphene nanocomposites; graphene (a,b), and surface-imidized graphene (c,d).

with different atomic composition and chain packing density of the rigid surface moieties.

CONCLUSIONS

Polyimide graphene nanocomposites were prepared using both reduced graphene and graphene surface modified with rigid imide moieties. Surface imidization was performed using a grafting method of step-by-step polycondensation from an amine-functionalized graphene. The storage tensile modulus of the nanocomposites increased with increasing graphene content linearly at 50 and 150 °C, whereas no effect on the glass transition temperature was observed. The modulus increase for nanocomposites containing surface-imidized graphene was 25−30% higher than with unmodified graphene. Both neat polyimide and polyimide nanocomposites exhibited shape memory behavior with a switching temperature of 230 °C. The recovery rate of the polyimide improved with addition of graphene. The morphology of the graphene in polyimide was studied under TEM.

EXPERIMENTAL SECTION

Materials. Bisphenol A dianhydride (BPADA), 3,3′,4,4′-biphenyl tetracarboxylic dianhydride (s-BPDA), 4,4′-bis(4-aminophenoxy) biphenyl (BAPP), and 2,2′-dimethyl-4,4′-diaminobiphenyl (*m*-tolidine) were purchased from Polyscience Inc., Chriskev, and Wakayama Seika Kogyo Co., respectively, and used without further purification. Toluene, chloroform, methanol, and *N*-methyl-2-pyrrolidone (NMP) were obtained from Sigma and used as received. Oxygenated graphene and reduced graphene were generously donated by Vorbeck Materials Corp.

Measurements. Thermal gravimetric analysis (TGA) was performed under a nitrogen atmosphere on a TA model 2950 using a heating rate of 10 °C min^{-1}. A Thermo Nicolet Nexus 470 ESP FT-IR was interfaced with the TGA instrument and used for characterization of any evolved gases. Modulus measurements were performed films using a TA Instruments model Q800 dynamic mechanical analyzer (DMA) in the tensile mode. Shape memory measurements were measured by model Q800 DMA by the following sequence: (i) increase the temperature to the switching temperature 230 °C with a ramp rate of 5 °C/min, (ii) apply mechanical deformation, ε_m, (iii) cool to 30 at 10 °C/min for 10 min and remove stress, and then cycles were repeated four times. The molecular weight distribution of the polymers was characterized by size exclusion chromatography (SEC) using a Waters Breeze System with three Styragel columns at 35 °C and a refractive index detector with a mixture of THF and 0.02 g/mL tri-*n*-octylamine. The molecular weight *versus* elution time was calculated using narrow polydispersity polystyrene standards. X-ray photoelectron spectroscopy (XPS) was performed using PHI-VERSAPROBE 5000 scanning microprobe with an Al Kα radiation (1486.6 eV) focused source with a 180° hemispherical electron energy analyzer. Survey scans were obtained by four passing sweeps of 93.3 eV over the sample. High-resolution spectra of C1 s and O1 s were obtained using a pass energy of 23.5 eV and dwell time of 0.8 s/data point for C1 s and 4.8 s/data point for O1 s. The atomic percentage ratio values were calculated from the high-resolution spectra, where the background signal-to-noise ratio of O1 s was 2.

Shirley background subtraction, shift of data sets based on 284.6 eV, atomic percentage based on survey scans, and peak deconvolution of high-resolution spectra were performed using Multipak software.

Surface Modification of Graphene. Highly oxygenated graphene nanosheets were dispersed in anhydrous THF (0.1 mg/cm^3) and sonicated to generate a homogeneous dispersion. *p*-Phenylene trimethoxyaminosilane (10:1, *p*-PTMAS/graphene) was added, and the resulting mixture was heated at reflux for 15 h. After cooling to room temperature, the aminophenyl-modified graphene was recovered by filtration, washed several times with THF, and allowed to air-dry in a vacuum oven. The resulting material was dispersed in anhydrous NMP (0.1 mg/cm^3) and sonicated for 15 min in flame-dried vessels. Dry s-BPDA anhydride (10:1) was added to the surface-functionalized graphene/NMP dispersion and heated at reflux with stirring for 15 h. The resulting mixture was allowed to cool to room temperature, and the solids were filtered, washed several times with NMP, and dried to provide graphene with a terminal anhydride functional end group. This process was repeated with addition of *m*-toldine (10:1) to the surface-functionalized graphene/NMP dispersion to obtain graphene with an imide surface modifier and amine end group. The imide surface-modified graphene in this study contains 4 units with amine end groups. Imide moieties were covalently attached to the graphene surface by adding diamine or dianhydride to the surface-modified graphene.

Neat Polyimide Polymerization. Polyimide was prepared according to our previously published method.[15] Briefly, dried BPADA (1 equiv) was added to a stirred solution of BAPP in anhydrous NMP mixed under dry N_2, and the resulting solution was allowed to stir for 24 h to obtain a high molecular weight poly(amic acid). The temperature of this solution was increased to reflux in NMP for 3 h to convert the poly(amic acid) to polyimide. The resulting polyimide was precipitated in methanol, filtered, washed several times with methanol to remove the NMP, and dried in a vacuum oven overnight.

Nanocomposite Film Casting. Polyimide graphene nanocomposites were prepared by sonication of graphene in chloroform for 3 h, and a solution of polyimide in chloroform was then added and the mixture sonicated for an additional 30 min. This dispersion of polyimide/graphene in chloroform ensured a minimum amount of solvent before casting to avoid reaggregation of the graphene. Films were air-dried overnight and further dried by a stepwise solvent removal in a vacuum oven from 80 to 170 °C over 7 days to ensure complete solvent removal. Nanocomposites with graphene loading levels of 0.05−8 wt % were prepared. Two types of graphene, reduced graphene and graphene surface imidized with s-BPDA and *m*-tolidine (rigid imidized, RI), were used.

Conflict of Interest: The authors declare no competing financial interest.

Acknowledgment. Funding for this research was provided by the Subsonics Fixed Wing Project, Fundamental Aeronautics Program under NASA Contract NNC07BA13B. C. Chuang is thanked for helpful suggestions and insights on polyimide chemistry. D. Hull of NASA GRC and Wayne Jennings of Case Western Reserve University are thanked for TEM and XPS support, respectively.

REFERENCES AND NOTES

1. Novoselov, K. S.; Geim, A. K.; Morozov, S. V.; Jiang, D.; Zhang, Y.; Dubonos, S. V.; Grigorieva, I. V.; Firsov, A. A. Electric Field Effect in Atomically Thin Carbon Films. *Science* **2004**, *306*, 666–669.
2. Geim, A. K.; Novoselov, K. S. The Rise of Graphene. *Nat. Mater.* **2007**, *6*, 183–191.
3. Geim, A. K. Graphene: Status and Prospects. *Science* **2009**, *324*, 1530–1534.
4. Geim, A. Random Walk to Graphene (Nobel Lecture). *Angew. Chem., Int. Ed.* **2011**, *50*, 6967–6985.
5. Geim, A. K.; Kim, P. Carbon Wonderland. *Sci. Am.* **2008**, *298*, 68–75.
6. Lee, C.; Wei, X.; Kysar, J. W.; Hone, J. Measurement of the Elastic Properties and Intrinsic Strength of Monolayer Graphene. *Science* **2008**, *321*, 385–388.
7. Gómez-Navarro, C.; Burghard, M.; Kern, K. Elastic Properties of Chemically Derived Single Graphene Sheets. *Nano Lett.* **2008**, *8*, 2045–2049.
8. Wilson, D.; Stenzenberger, H. D.; Hergenrother, P. M. *Polyimides*; Chapman & Hall: London, 1990.
9. Delozier, D. M.; Watson, K. A.; Smith, J. G., Jr.; Clancy, T. C.; Connell, J. W. Investigation of Aromatic/Aliphatic Polyimides as Dispersants for Single Wall Carbon Nanotubes. *Macromolecules* **2006**, *39*, 1731–1739.
10. Wang, D. H.; Arlen, M. J.; Baek, J.-B.; Vaia, R. A.; Tan, L.-S. Nanocomposites Derived from a Low-Color Aromatic Polyimide (CP2) and Amine-Functionalized Vapor-Grown Carbon Nanofibers: *In Situ* Polymerization and Characterization. *Macromolecules* **2007**, *40*, 6100–6111.
11. Wu, S.; Hayakawa, T.; Kakimoto, M.-a.; Oikawa, H. Synthesis and Characterization of Organosoluble Aromatic Polyimides Containing POSS in Main Chain Derived from Double-Decker-Shaped Silsesquioxane. *Macromolecules* **2008**, *41*, 3481–3487.
12. Park, C.; Smith, J. G., Jr.; Connell, J. W.; Lowther, S. E.; Working, D. C.; Siochi, E. J. Polyimide/Silica Hybrid-Clay Nanocomposites. *Polymer* **2005**, *46*, 9694–9701.
13. Cheng, C.-F.; Cheng, H.-H.; Cheng, P.-W.; Lee, Y.-J. Effect of Reactive Channel Functional Groups and Nanoporosity of Nanoscale Mesoporous Silica on Properties of Polyimide Composite. *Macromolecules* **2006**, *39*, 7583–7590.
14. Southward, R. E.; Thompson, D. W. Metal−Polyimide Nanocomposite Films: Single-Stage Synthesis of Silvered Polyimide Films Prepared from Silver(I) Complexes and BPDA/4,4′-ODA. *Chem. Mater.* **2004**, *16*, 1277–1284.
15. Lebron-Colon, M.; Meador, M. A.; Gaier, J. R.; Sola, F.; Scheiman, D. A.; McCorkle, L. S. Reinforced Thermoplastic Polyimide with Dispersed Functionalized Single Wall Carbon Nanotubes. *ACS Appl. Mater. Interfaces* **2010**, *2*, 669–676.
16. Israelachvili, J. N. *Intermolecular Surface Forces* 3rd ed.; Academic Press: San Diego, CA, 2006.
17. Behl, M.; Lendlein, A. Shape-Memory Polymers. *Mater. Today* **2007**, *10*, 20–28.
18. Liu, C.; Qin, H.; Mather, P. T. Review of Progress in Shape-Memory Polymers. *J. Mater. Chem.* **2007**, *17*, 1543–1558.
19. Koerner, H.; Kelley, J.; George, J.; Drummy, L.; Mirau, P.; Bell, N. S.; Hsu, J. W. P; Vaia, R. A. ZnO Nanorod−Thermoplastic Polyurethane Nanocomposites: Morphology and Shape Memory Performance. *Macromolecules* **2009**, *42*, 8933–8942.
20. Khonakdar, H. A.; Jafari, S. H.; Rasouli, S.; Morshedian, J.; Abedini, H. Modeling of Shape Memory Induction and Recovery in Heat-Shrinkable Polymers. *Macromol. Theory Simul.* **2007**, *16*, 43–52.
21. Dong, J.; Weiss, R. A. Shape Memory Behavior of Zinc Oleate-Filled Elastomeric Ionomers. *Macromolecules* **2011**, *44*, 8871–8879.
22. Jeon, H. G.; Mather, P. T.; Haddad, T. S. Shape Memory and Nanostructure in Poly(norbornyl-POSS) Copolymers. *Polym. Int.* **2000**, *49*, 453–457.
23. Xiao, X.; Xie, T.; Cheng, Y.-T. Self-Healable Graphene Polymer Composites. *J. Mater. Chem.* **2010**, *20*, 3508–3514.
24. Xie, T. Recent Advances in Polymer Shape Memory. *Polymer* **2011**, *52*, 4985–5000.
25. Schniepp, H. C.; Li, J.-L.; McAllister, M. J.; Sai, H.; Herrera-Alonso, M.; Adamson, D. H.; Prud'homme, R. K.; Car, R.; Saville, D. A.; Aksay, I. A. Functionalized Single Graphene Sheets Derived from Splitting Graphite Oxide. *J. Phys. Chem. B* **2006**, *110*, 8535–8539.
26. Schniepp, H. C.; Kudin, K. N.; Li, J.-L.; Prud'homme, R. K.; Car, R.; Saville, D. A.; Aksay, I. A. Bending Properties of Single Functionalized Graphene Sheets Probed by Atomic Force Microscopy. *ACS Nano* **2008**, *2*, 2577–2584.
27. McAllister, M. J.; Li, J.-L.; Adamson, D. H.; Schniepp, H. C.; Abdala, A. A.; Liu, J.; Herrera-Alonso, M.; Milius, D. L.; Car, R.; Prud'homme, R. K.; *et al.* Single Sheet Functionalized

Graphene by Oxidation and Thermal Expansion of Graphite. *Chem. Mater.* **2007**, *19*, 4396–4404.
28. Yoonessi, M.; Gaier, J. R. Highly Conductive Multifunctional Graphene Polycarbonate Nanocomposites. *ACS Nano* **2010**, *4*, 7211–7220.
29. Wolfe, W. L., Zissis, G. J. *The Infrared Handbook*; Environmental Research Institute of Michigan Ann Arbor Infrared Information and Analysis Center, Office of Naval Research: Washington, DC, 1978.
30. Xia, Q.; Wang, B.; Wu, Y. P.; Luo, H. J.; Zhao, S. Y.; van Ree, T. Phenyl Tris-2-methoxydiethoxy Silane as an Additive to PC-Based Electrolytes for Lithium-Ion Batteries. *J. Power Sources* **2008**, *180*, 602–606.
31. Mittal, K. *Polyimides: Synthesis, Characterization, and Applications*; Springer: New York, 1984.
32. Russat, J. Characterization of Polyamic Acid Polyimide Films in the Nanometric Thickness Range from Spin Deposited Polyamic Acid. *Surf. Interface Anal.* **1988**, *11*, 414–417.